University of Groningen
Faculty of Mathematics and Natural Sciences
TopMaster Programme in Nanoscience

Magdalena Wojtaszek

s 1711385

Superlattices as building blocks for quantum cascade lasers: a theoretical analysis of superlattice states

Review paper

Supervised by:
Dr. Victor Malyshev
Theorie van de Gecondenseerde Materie
Zernike Institute for Advanced Materials

June 2008

Abstract

The work presents a review of theoretical approaches to describe superlattice states and point out the importance of its teoretical investigations for infrared applications (especially quantum cascade lasers). The paper zoom in the fundamental concepts, to which most of the scientific theoretical publications refer to, but in which detailed derivation is usually omitted. Nearly 40 years of investigations, however, brought the considerations of physical phenomena in superlattices to quite sophisticated level, difficult to master for inexperienced reader. In particular, the paper provides a detailed description of $\boldsymbol{k}\cdot\boldsymbol{p}$ method for bulk materials and its extension to superlattices. Furthermore, basing on the envelope function approach and the transition matrix formalism, the formation of minibands is viewed. At the end, the Wannier states and its extension to the Wannier-Stark states, to describe systems with an applied external electric field, are briefly discussed.

Contents

List of Figures

Chapter 1

Band-gap engineering for infrared technology

Low-dimensional electron systems based on semiconductors nanostructures are one of the most exciting areas in solid state physics. The present report focuses on properties of semiconductor superlattices, which, since the pioneer paper of Esaki and Tsu almost 40 years ago (see [1]), have been the subject of enormous theoretical and experimental activity, especially within the so called *band-gap engineering*. Since the electronic structure of a superlattice depends on the layer thickness (precisely controlled), on the number of fabricated layers and on the type of constituent materials, then their important intrinsic properties, such as energy bands and effective mass, can be readily modified. This leads to big flexibility in designing the electronic band structure of superlattices. Apart from being a great object for fundamental investigations of quantum phenomena, superlattice structures opened perspectives to many useful technological applications (especially for high-speed, high-mobility structures, vertical transport devices, sequential tunneling structures, including superlattice lasers, electro-optical modulators, and infrared avalanche photodetectors) mostly operating in infrared - the spectral region, which still is poorely developed.

1.1. Standard laser operation principle for mid-infrared technology: limitations

The operating characteristics of present day mid-infrared laser diodes at wavelengths greater than 3 μm, exploiting recombination across the bandgap, lag still far behind near-infrared laser diodes, due to several obstales. First of all, there exist just a few compatible narrow-gap semiconductors, which could be used for this purpose. Moreover, they experience many intrinsic material limitations. The best known of these is the nonradiative Auger recombination, where nonequilibrium electron-hole pairs recombine, transfering the energy and momentum to another carrier rather than emitting a photon.

The primary consequence of the Auger recombination is that, left alone, the nonequilibrium carrier density of upper state would be rapidly depleted, and large driving currents are required to replenish the carrier density to sustain laser action. The Auger recombination becomes exponentially more important as the wavelength increases. Approximate analytic forms describing the intrinsic Auger recombination process for bulk semiconductors with valence electron mass m_v much greater than condution electron mass m_c, $m_v \gg m_c$,

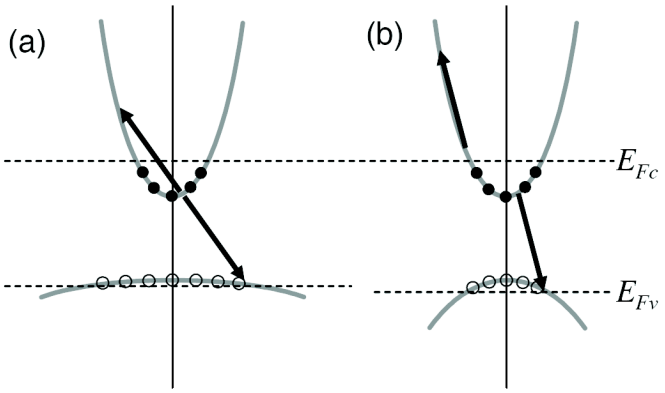

Figure 1.1: Auger recombination describes the process in which a conduction electron recombines with a heavy hole, and transfers the excess energy to another conduction electron. This process is much more efficient for materials with heavy valence band mass (a) because in these materials carriers spread in $\boldsymbol{k}$-space to a larger extent than in the case of a light hole mass (b). Therefore, the top of the band in case (a) is much more occupied than in case (b), and the conservation of energy and momentum during nonradiative recombination with a carrier near band edge in conduction band is easy to satisfy (efficiency increases with the increase of occupation state imbalance). In case (b), on the contrary, it is not possible to complete the transition without using at least one carrier that is in the exponential tail of the distribution.

indicate that the recombination probability depends exponentially on the fundamental energy gap $\propto exp(-AE_g/k_BT)$, where the coefficient A varies from 0 to 0.5. Moreover, it is also influenced by density of states imbalance (see Fig. 1.1). In the 3-5 μm range many of the materials have spin-orbit splittings, with an energy comparable to the band gap, which provides an additional channel for the Auger recombination. Thus, for narrow-gap semiconductors the Auger recombination is a problem of greater importance than it would be for semiconductors emitting in the optical wavelength. This makes the operation of laser diodes within the 3-30 μm wavelength range significantly more difficult than for near-infrared wavelengths. The advent of superlattices, however, brought a new mechanism for photon generation, which would revolutionize devices in the spectral region between well advanced microwave fast semiconductor electronics and visible region devices (with well developed optical technology).

1.2. Alternative operating principle: Quantum Cascade Laser

Intrinsic limitations of the radiative recombination in the mid-infrared region forced scientists to look for operating principles, which differ from those for standard lasers. A novel approach has led to developing Quantum Cascade Lasers (QCL), firstly demonstrated by Faist, Capasso, Sirtori and colleagues in 1994. The core of QCL consist of a multiquantum-well (MQW) structure made up of repeated stages of active regions sandwiched between electron-injecting and -collecting regions, both parts built as superlattices. When a proper bias is applied, an "electron cascade" - intersubband (between subbands of the same quantum well) or interminiband (between minibands of adjacent quantum wells) transitions occur. The injector acts as a reservoir of electrons for the injection into the active region of the next stage. It also acts as a collector of electrons from the preceding active region.

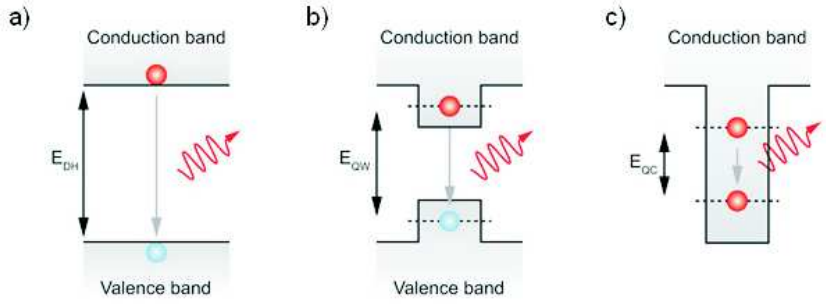

Figure 1.2: The three basic schemes for the photon emission is semiconductors, highlighting bipolar, (a) and (b), and unipolar, (c), operations. (a) Interband emission by the recombination across the bandgap (standard lasers). (b) Interband emission by the recombination between confined states in quantum wells. (c) Intraband emission by the transition between subbands within one quantum well.

Standard semiconductor lasers operate thanks to population inversion, where population of conduction band is higher than of valence band, and output photon-beam is generated through the recombination of electron-hole pairs (interband transition). Radiative recombination can be enhanced by stimulated emission. Hence, in properly designed cavity, once emitted photon can initiate further emissions, by traveling through gain medium several times. Contrary to standard lasers, the emission in QCL involves just one type of carriers (usually electrons from conduction band). Because of that we say that QCL is unipolar (see Fig. 1.3).

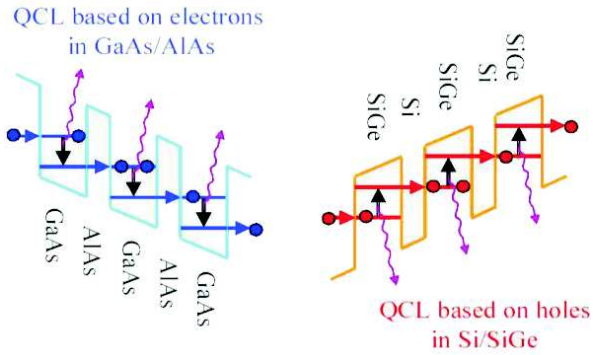

Figure 1.3: Two types of carrier transport in unipolar quantum cascade lasers, the one based on electrons (transitions in conduction bands) and the other one based on holes (transitions in valence bands)

The transitions in active regions are tuned by an applied external electric field, so that the outcoming photon's energy is not constrained by energy gap of specific material (tunability). Additionally, while in semiconductor laser diodes, electrons and holes are recombining across the band gap and play no further role in photon generation, in unipolar QCL, once an electron has undergone an intersubband transition and emitted a photon, it tunnels into the next period

of the structure, where it can emit another photon. The process of emission of multiple photons by single electron tunneling through the QCL structure gives rise to the name *cascade*. It makes the quantum efficiency of QCL much higher than in semiconductor laser diodes and independent from the size of the cavity, therefore is very promising for designing mid-infrared coherent light sources.

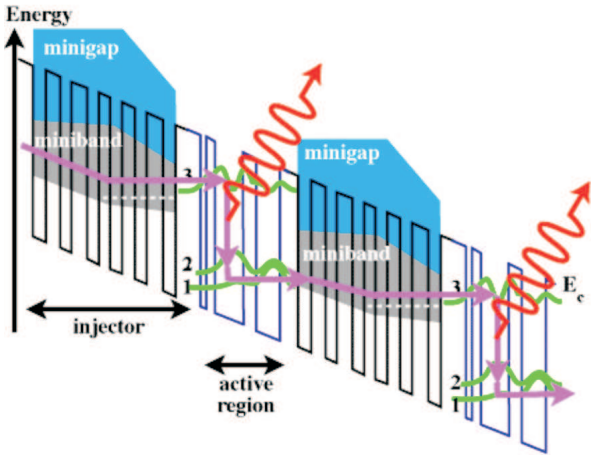

Figure 1.4: Cross-section of a Quantum Cascade Laser structure and a schematic illustration of operating principle, with indication of superlattice injecting/collecting region and a 3-quantum-well (3QW) active region. Violet arrows show direction of the electrons flow, red arrows indicate the radiative transition, green lines point out the wavefunctions corresponding to the levels in active region. One carrier, when going through structure consisting of N periods of the injector/active region, produces N photons.

The electron transport through a QCL structure is a complicated interplay between the relaxation through light emission and scattering in the active region, as well as the transmission through tunneling and scattering in the injector/collector region.

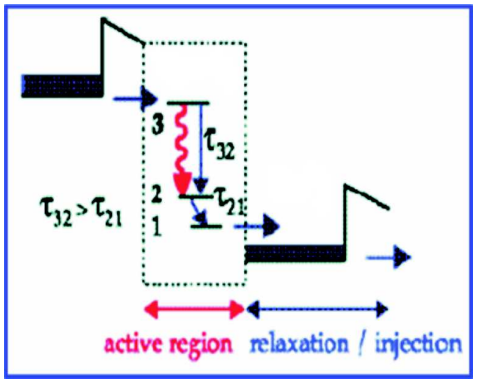

Figure 1.5: Schematic illustration of recombination in the active region of QCL (3 level system). The population inversion condition obeys under a relation $\tau_{32} > \tau_{21}$, where τ_{if} is the electron scattering time from an initial subband level i to a final subband level f.

Suitable design of layer thicknesses determines the electron wave functions of the subbands in the superlattice and tailors scattering rates. The scattering rate between two sub-

bands is strongly dependents upon the overlap of the wave functions and on the energy spacing between the subbands. In order to decrease the average intersubband scattering rate $W_{32} = \frac{1}{\tau_{32}}$, and hence increase the population inversion, the overlap of the upper and lower laser levels is reduced. This is often achieved through designing the layer thicknesses such that the upper laser level is mostly localised in the left-hand well of the 3QW active region, while the lower laser level wave function is made to mostly reside in the central and right-hand wells. This is known as a *diagonal* transition. A *vertical* transition is the one when the upper laser level is predominantly localized in the central and right-hand wells. This increases the wave function overlap and W_{32}, and as a result reduces the population inversion. However, at the same time the strength of the radiative transition, and therefore the gain, grows. In order to increase W_{21}, the lower laser level and the ground level wave functions are designed in such a way that they have a good overlap. To further push up W_{21}, the energy spacing between the subbands is designed such that it is equal to the longitudinal optical (LO) phonon energy ($\sim 36\ meV$ in $GaAs$). Then, the resonant LO phonon-electron scattering can quickly depopulate the lower laser level (level 2 at Fig. 1.5). All these mechanisms can be analyzed in terms of rate equations (phenomenological approach). An important issue is the transport of electrons from the injector into the upper laser state (when an electron doesn't recombine in active region but escapes to the upper miniband of the collector). The optimum design strategies try to enhance the injector-active-region coupling via resonant tunneling and, at the same time, to prevent the carriers from propagating into the continuum.

Although the design and production of these structures have reached a high degree of sophistication, the direct experimental verification on the microscopic mechanisms is still poor. From a theoretical point of view, the degree of coherence in quantum transport (resonant tunneling vs. nonresonant incoherent transport) is determined by the interplay between electron wave packet propagation and dissipative scattering processes. Thus, a detailed investigation of the ultrafast gain dynamics provides better insight into the QCL physics.

Chapter 2

Superlattices - the keystone for designing mid-infrared devices

To understand the performance of QCL, we first need to have a detailed insight into electronic properties of it's main building block - superlattice. Superlattices are completely man-made heterostructures, grown through periodically repeated deposition of layers of different semiconductor materials on the top of each other in the growth direction: they represent a repeated sequence of quantum barriers and wells. Development of growth techniques [esp. molecular beam epitaxy (MBE) and metal-organic chemical vapor deposition (MOCVD)] allows one to control the thicknesses of these layers with a high precision, so that the interfaces are well defined within one atomic monolayer. Periodic arrangement of layers in superlattice (with period d) imply periodic potential profile, as positions of the bottom of the conduction band and of the top of the valence band vary from material to material (see Fig 2.3).

Among these structures, we distinguish two groups: compositional and doping superlattices. Doping superlattices consist of alternating n- and p-type layers of the same semiconductor, in which charged dopants modulate the electronic potential. Compositional superlattices consist of alternating layers of two different semiconductors. Materials to form a heterostuctured superlattice are chosen to have similar lattice constants, like for example GaAs and AlAs, to provide a stable (and hence precise) growth of layers.

The term *superlattice* refers to any type of periodic structure, including both multiple quantum well systems and true superlattices with strong inter-well coupling. As indicated on Fig. 2.2, in multi-quantum well system, wells are well separated by thick barriers, and therefore the overlap of wavefunctioncs from adjacent wells is very small: there is no coupling between states within the wells, and no significant tunneling current. Energy levels are discrete. The tunneling current through such a structure is very inefficient, and technological applications are very limited. In the report, the clear distinction between both cases will be kept and the term *superlattice* will only be related to structures of strong inter-well coupling.

Typically the width d of a single layer of material in SL ranges from several to tens of monolayers, $d \gg a$ (a - lattice constant of a solid material) and the basis is repeated tens times. The composition variation modulates the electronic potential on a length scale shorter than an electron mean free path. This, in turn, leads to a significant wavefunction overlap and coherent electron transport in growth direction, which, as mentioned before, distinguish superlattices from so called multi-quantum-wells structures.

Coupling between states and periodic potential profile gives rise to formation of energy

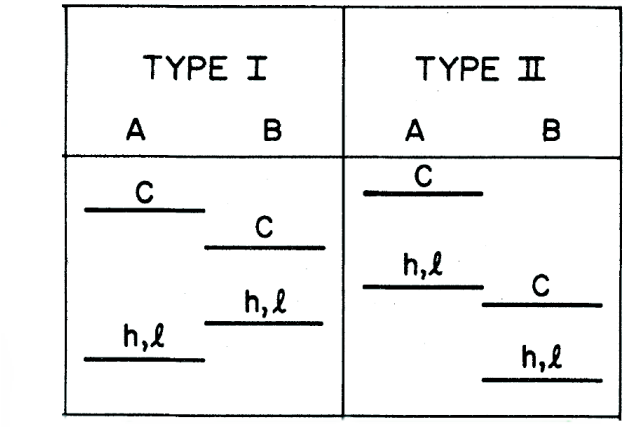

Figure 2.1: In case of SL we distinguish two basic lineups of conduction and valence band. In type I both, the conduction and valence bands of one of the components, are inside the energy gap of second material, while in type II bi-component structure both, conducting and valence bands, are shifted up (or down) with respect to bands of the second material layer. Labels c, h, and l indicate the conduction, heavy hole, and light hole bands, respectively.

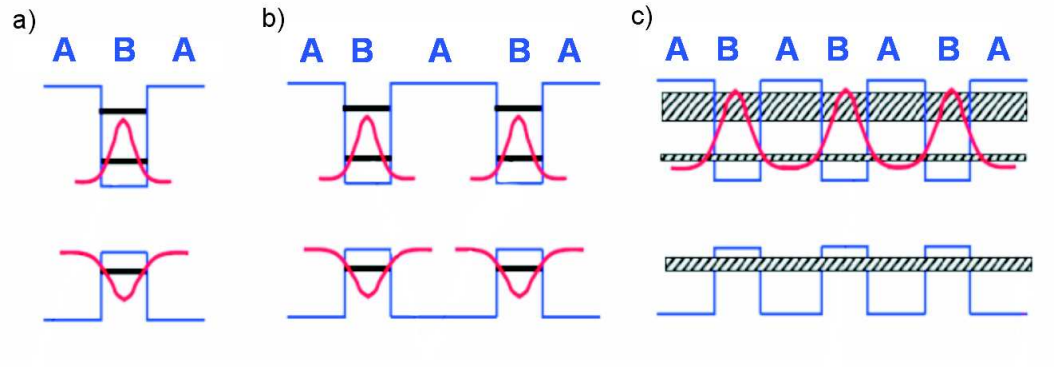

Figure 2.2: A schematic diagram of differences between a multi-quantum-well system and a superlattice. A single quantum well (a) is characterized by discrete levels, in a multi-quantum-well system (b) the wavefunctions of adjacent wells barely overlap, and therefore interactions between them are very weak (weak coupling). In a superlattice (c) we have the strong overlap of states, which leads to formation of minibands

bands like in a crystal, but here the energy width Δ of the band as well as the extension of the Brilliouin zone are much smaller than analogous values for a conventional conduction band (as $\frac{2\pi}{d} \ll \frac{2\pi}{a}$). Thus, in the case of superlattices we are talking about *minibands* (see Fig. 2.3).

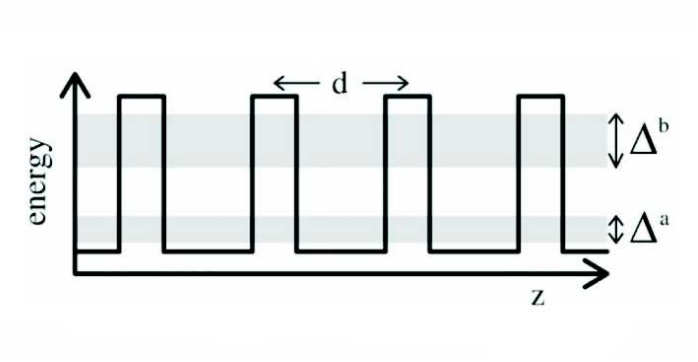

Figure 2.3: Formation of minibands across the periodic structure of SL. The solid line indicates potential profile, the gray fields indicate minibands. The most extensively studied superlattice consist of $GaAs/Ga_{1-x}Al_xAs$, having a very small lattice-constant mismatch (0.08% between $GaAs$ and $Ga_{0.5}Al_{0.5}As$) and hence a structure is not significantly strained. The band gap of $GaAs$ is smaller than that of $Ga_{1-x}Al_xAs$. Therefore, in the $GaAs/Ga_{1-x}Al_xAs$ heterojunction, the conduction band-edge of $GaAs$ lies at a lower energy than the conduction-band edge in $Ga_{1-x}Al_xAs$. Thus, the GaAs acts as a quantum well and the $Ga_{1-x}Al_xAs$ as a potential barrier both for electrons and holes.

Electronic states of small energy, whose mean free path is much less than the thickness of the constituent material layers, are essentially kinetically confined within the layer of a particular material. Such states, therefore, are not much modified by superlattice potential modulation. On the other hand, electronic states, whose mean free path is comparable to or longer than the thickness of the constituent material layers, are significantly influenced by the spatial potential modulation of the superlattice. As a result, those electronic states, which are relatively close in energy to the band edges (having relatively long life-times and long mean free paths) are of the primary interest in SL materials. Thus, the teories of the superlattice electronic structure are basically band-edges theories (they consider just a few states close to the band edge), and take into account perturbations just within comparable energy range, such as the spin-orbit interactions, lattice strain and electric fields.

2.1. Electronic band structure of a superlattice

The electronic band structure of any quantum system is directly related to many macroscopic properties of the material and therefore it is a matter of large interest. A very wide range of theoretical techniques has been applied to SL electronic structure calculations, starting from atomistic *ab initio* methods to *ad hoc* (heuristic) methods, applicable to only specific material system. Among those methods, the most important are: tight-binding calculations, pseudopotential calculations, and the one mostly explored: envelope-function technique for restricted basis set (obtained from the $\boldsymbol{k} \cdot \boldsymbol{p}$ method). The degree of complexity in these approaches ranges from scaled Kronig-Penney models (describing an electron in a 1D rectangular

potential) to self-consistent many-electron calculations. Obviously, a choice of particular theoretical approach depends both on a material system studied and on a question asked about it. For example, a $GaA/Ga_{1-x}Al_xAs$ superlattice is relatively easy to describe theoretically, as both component materials have direct band-gap, their lattice constants match very well, and the relative band-gap difference of these two materials is big, giving just a weak mixing of constituent material bands. For more complex materials systems, like those with small-band-gap, or type II band lineup, where the band mixing may become important, more sophisticated theoretical approaches are necessary.

The Hamiltonian of the superlattice to study, $\hat{H}$, can be separated into two parts: $\hat{H} = \hat{H}_0 + \hat{H}_{scatt}$, where $\hat{H}_0$ contains the parts with superlattice potential and a static electric field E applied in the growth direction, i.e., $\hat{H}_0 = \hat{H}_{SL} + \hat{H}_E$. The Hamiltonian $\hat{H}_{scatt}$ describes the scattering processes, in which we may include interface roughness, impurity, and electron-phonon scattering processes, which opens the route for the carrier-lattice system to move towards thermal equilibrium.

Apart from defining the Hamiltonian, we also have to describe the states of the system and their properties. The most common strategy to describe electronic structure of SL is to make use of the knowledge we have about constituent bulk materials. Usually, it is assumed that the intrinsic parameters of the bulk material (like effective mass of carriers) do not change when materials are combined to form the SL. However, the interface region description has to be taken into account. In particular, in tight-binding models, the matrix elements between orbitals on near-neighbor atoms at opposite sides of the interface must be specified (see Ref. [2]).

Although the physical results obtained from the theory should be independent of the specific choice of basis functions, there are different advantages and drawbacks (like computational complexity) connected to a given choice. Different approximations as well as different quantities of interest suggest different choice of basis states. Therefore a good choice of basis states is a crucial question. Possible choices are: *(i)* Bloch functions, being the eigenstates of the bare superlattice potential $\hat{H}_{SL}$, which are spatially extended across the whole structure; *(ii)* Wannier functions, which may be constructed from Bloch states, but so that they are spatially well localized; *(iii)* Wannier-Stark states which are eigenstates of $\hat{H}_0$, the Hamiltonian of the superlattice potential plus the applied electric field E. The second choice is especially useful, as spatial localization of the Wannier states enables one to setup a picture of transport in which scattering occurs from one spatial region of the structure to another. The Wannier functions do not depend on bias. This is computationally advantageous because coupling matrix elements between Wannier functions may be calculated only once, and then the same matrix elements may be used at any applied bias. A disadvantage in using this basis is that the Wannier functions are not eigenstates of the superlattice Hamiltonian $\hat{H}_0$, and it is therefore difficult to obtain a physical interpretation in the energy picture.

Chapter 3

Envelope function formalism for SL

On the basis of empirical knowledge about constituent materials, we can describe a SL introducing concept of periodicity, as in conventional band-structure methods (the Bloch theorem), but for a larger unit cell (superlattice cell). Historically, this approach was the first one to study the superlattice band structure, and was a starting point for many approximations, one of the most important among which (and still explored) is the envelope function approximation (EFA). The EFA is basically an extention of the effective-mass equation of the $\boldsymbol{k}\cdot\boldsymbol{p}$ method, used in the theory of bulk semiconductures, to SL. As the $\boldsymbol{k}\cdot\boldsymbol{p}$ theory is particularly effective in describing the states near the conduction- and valence-band edges, it is natural to attempt applying it to the SL. This allows us to reduce the problem of solving the Hamiltonian for wavefuntions to the problem of solving a set of second-order differential equations for envelope functions. The essence of the $\boldsymbol{k}\cdot\boldsymbol{p}$ method is in restricting to low energies, and therefore in considering the limited number of bulk states in the electronic structure basis.

3.1. $\boldsymbol{k}\cdot\boldsymbol{p}$ Method for Bulk Materials

The $\boldsymbol{k}\cdot\boldsymbol{p}$ method was developed by J. M. Luttinger and W. Kohn (see [3]) in order to generalize the effective mass approximation for the description of degenerate bands, or bands with band extrema not at the center of the Brillouin zone (non-direct band gap systems). This generalization was necessary in order to be able to calculate the band structures of materials like Si or Ge. In $\boldsymbol{k}\cdot\boldsymbol{p}$ approaches, rather than trying to solve for the energy levels and wavefunctions directly from an approximation of crystal potentials, one starts with experimental values for the energy levels and the momentum matrix elements at zone center. The only necessary experimental parameters are the band edge energy gaps and momentum matrix elements of constituent materials, which can be readily deduced from experimental studies (e.g., photoluminescence, absorption, and effective-mass measurements). The energy level structure and matrix elements throughout the zone follow directly from the known symmetry of the band-edge states and the Schrödinger equation.

The starting point for the $\boldsymbol{k}\cdot\boldsymbol{p}$ method is the time-independent, single-particle Hamiltonian in the coordinate representation:

$$\hat{H}(r) = \frac{\hat{\boldsymbol{p}^2}}{2m} + \frac{\hbar}{4m^2c^2}[\boldsymbol{\sigma}\times\nabla V(\boldsymbol{r})]\cdot\hat{\boldsymbol{p}} + V(\boldsymbol{r}), \tag{3.1}$$

where $\hat{p}$ is the momentum operator, $\boldsymbol{\sigma}$, are the Pauli matrices, and $V(\boldsymbol{r})$ is the crystal potential. The second term in Eq. 3.1 represents the spin-orbit interaction. The spin-orbit coupling can be combined with the crystal potential term into an effective potential, $\bar{V}(\boldsymbol{r})$, so that

$$\hat{H}(r) = \frac{\hat{\boldsymbol{p}}^2}{2m} + \bar{V}(\boldsymbol{r}). \tag{3.2}$$

The eigenvalues and eigenfunctions are found from:

$$\hat{H}(\boldsymbol{r})|l\boldsymbol{k}> = E_l(\boldsymbol{k})|l\boldsymbol{k}>, \tag{3.3}$$

where $|l\boldsymbol{k}>$ is the bulk wavefunction for a particle in band l with wavevector $\boldsymbol{k}$, $E_l(\boldsymbol{k})$ is the energy of the state.

Let's assume that we know the band energies and eigenstates at the momentum value $\boldsymbol{k}_0 = 0$ (in the same way we procede for $\boldsymbol{k}_0 \neq 0$) and we want to compute the states in vicinity of $\boldsymbol{k}_0$. The states $|l\boldsymbol{k}>$ cannot be directly expanded in terms of $|n\boldsymbol{k}_0>$, because these functions are orthogonal to each other for $\boldsymbol{k} \neq \boldsymbol{k}_0$. However, since the states for each $\boldsymbol{k}$ are complete, we can take it as a basis and write:

$$< \boldsymbol{r}|l\boldsymbol{k}> = e^{i\boldsymbol{k}\cdot\boldsymbol{r}} \sum_{n'} c_{ln'}(\boldsymbol{k}) < \boldsymbol{r}|n'\boldsymbol{0}> . \tag{3.4}$$

Here $c_{ln'}(\boldsymbol{k})$ is the expansion coefficient and the summation runs over all zone-center states. It is important to note that we will never need to solve or otherwise determine the bulk zone-center wavefunctions, because the requirements to proceed with $\boldsymbol{k}\cdot\boldsymbol{p}$ theory are the zone-center energy levels and momentum matrix elements, deduced from experimental measurements. If $< \boldsymbol{r}|n\boldsymbol{k}_0>$ is periodic with respect to the translation by a lattice vector $\boldsymbol{R}$, then $< \boldsymbol{r}|n\boldsymbol{k}>$ is also periodic (Bloch condition $< \boldsymbol{r}|l\boldsymbol{k}> = < \boldsymbol{r}+\boldsymbol{R}|l\boldsymbol{k}>$ is fulfilled).

The expansion in Eq. 3.4 can be substituted into the eigenvalue equation, (Eq. 3.3). Expanding the momentum operator yields

$$\sum_{n'} c_{ln'}(\boldsymbol{k}) \Big[\big(\frac{\hat{\boldsymbol{p}}^2}{2m} e^{i\boldsymbol{k}\cdot\boldsymbol{r}}\big)|n'0> + \big(\frac{\hat{\boldsymbol{p}}}{m} e^{i\boldsymbol{k}\cdot\boldsymbol{r}}\big) \cdot \big(\hat{\boldsymbol{p}}|n'0>\big) + e^{i\boldsymbol{k}\cdot\boldsymbol{r}} \big(\frac{\hat{\boldsymbol{p}}^2}{2m} + \bar{V}(\boldsymbol{r})\big)|n'0> \Big] = E_l(\boldsymbol{k}) e^{i\boldsymbol{k}\cdot\boldsymbol{r}} \sum_{n'} c_{ln'}(\boldsymbol{k})|n'0>, \tag{3.5}$$

where $\hat{\boldsymbol{p}} = -i\hbar\nabla$.

Multiplying both sides on the left with $e^{-i\boldsymbol{k}\cdot\boldsymbol{r}} <n,0|$ reduces the expression to:

$$\sum_{n'} c_{ln'}(\boldsymbol{k}) \Big[\frac{\hbar^2 k^2}{2m}\delta_{nn'} + \frac{\hbar\boldsymbol{k}}{m} <n0|\hat{\boldsymbol{p}}|n'0> + <n0|\frac{\hat{\boldsymbol{p}}^2}{2m} + \bar{V}(\boldsymbol{r})|n'0> \Big] = E_l(\boldsymbol{k}) \sum_{n'} c_{ln'}(\boldsymbol{k})\delta_{nn'}.$$

If eigenstates of the total angular momentum are used as a basis for the bulk wavefunctions, then the bulk energy forms a diagonal matrix, whose diagonal terms are the energies of the bulk states at zone center. In this basis, Eq. 3.6 reads:

$$\sum_{n'} c_{ln'}(\boldsymbol{k}) \Big[\big(\frac{\hbar^2 k^2}{2m} + E_n(0)\big)\delta_{nn'} + \frac{\hbar\boldsymbol{k}}{m}\boldsymbol{P}_{nn'}(0) \Big] = E_l(\boldsymbol{k}) c_{ln}(\boldsymbol{k}), \tag{3.6}$$

where

$$E_n(0) = <n0|\frac{p^2}{2m} + \bar{V}(\boldsymbol{r})|n0>, \tag{3.7}$$

$$\boldsymbol{P}_{nn'}(0) = <n0|\boldsymbol{p}|n'0> . \tag{3.8}$$

The properties of the zone-center wavefunctions only appear via the zone-center energies and momentum matrix elements. The more detailed structure of the wavefunctions themselves need not be known. Eq. 3.6 can be written in more compact way as:

$$\sum_{n'} M_{n'n}(\boldsymbol{k}) c_{n'l}(\boldsymbol{k}) = E_l(\boldsymbol{k}) c_{nl}(\boldsymbol{k}), \tag{3.9}$$

where the matrix M is the transpose of the term in square brackets in Eq. 3.6. This matrix is referred to as the $\boldsymbol{k}\cdot\boldsymbol{p}$ matrix. Its eigenvalues are the state energies at wavevector $\boldsymbol{k}$ and its eigenvectors are the coefficients relating any finite-$\boldsymbol{k}$ state to the zone-center states.

Until this step, the solution is exact. To make the problem tractable, a finite set of zone-center states is used to approximate the infinite basis set. This embodies the low-energy approximation involved in the $\boldsymbol{k}\cdot\boldsymbol{p}$ approach. For narrow-gap III-V materials, a minimal set of states includes the conduction band, heavy-hole, light-hole, and split-off band. Because each of these bands is degenerated at zone center, a total of eight bands are utilized and this approximation is referred to as 8-band $\boldsymbol{k}\cdot\boldsymbol{p}$ method. Unfortunately, the electronic structure generated by these eight bands has spherical symmetry [i.e., $E(\boldsymbol{k})$ depends only on $|\boldsymbol{k}|$] rather than having the proper cubic symmetry, and it is also inversion symmetric [i.e. $E(\boldsymbol{k}) = E(-\boldsymbol{k})$]. Inversion asymmetry and the reduction from spherical to cubic symmetry are consequences of the coupling of the eight band-edge states with the six antibonding p-like states. This fact is sometimes included by incorporating some of the effects of the antibonding p-states or by taking more band states.

Figure 3.1 shows the band structure of InAs (the dominant source of the conduction state in InAs/GaSb materials) calculated in 8-band $\boldsymbol{k}\cdot\boldsymbol{p}$, 14-band $\boldsymbol{k}\cdot\boldsymbol{p}$, and non-local pseudopotential models (after [12] and [15]). Whereas $\boldsymbol{k}\cdot\boldsymbol{p}$ models agree well with experiment near the zone-center (by choice of parameters), the error increases as the zone boundary is approached.

3.2. $\boldsymbol{K}\cdot\boldsymbol{p}$ Method for Heterostructures

The presented above $\boldsymbol{k}\cdot\boldsymbol{p}$ formalism can be straightforwardly expanded to cover also superlattice systems (see Chap. 3 in Ref. [6]. In order to distinguish between superlattice and bulk states, we use uppercase variables (L, N, and $\boldsymbol{K}$) for superlattice parameters and lowercase variables (l, n, and $\boldsymbol{k}$) for bulk parameters.

Application of the Hamiltonian from Eq. 3.2 to a superlattice wavefunction gives

$$H(\boldsymbol{r}) <\boldsymbol{r}|L,\boldsymbol{K}> = E_L(\boldsymbol{K}) <\boldsymbol{r}|L,\boldsymbol{K}>, \tag{3.10}$$

where $|L,\boldsymbol{K}>$ is the superlattice wavefunction for a particle in band L with superlattice wavevector $\boldsymbol{K}$, and $E_L(\boldsymbol{K})$ is the state energy.

The effective potential $\bar{V}$ from Eq. 3.2, now consists of a periodic potential of the crystal, V_0, and confinement potential V_{conf}, which arise from the band offsets for the conduction and valence band edges across an interface (effect of the mismatch of the bandgaps). Hence, the

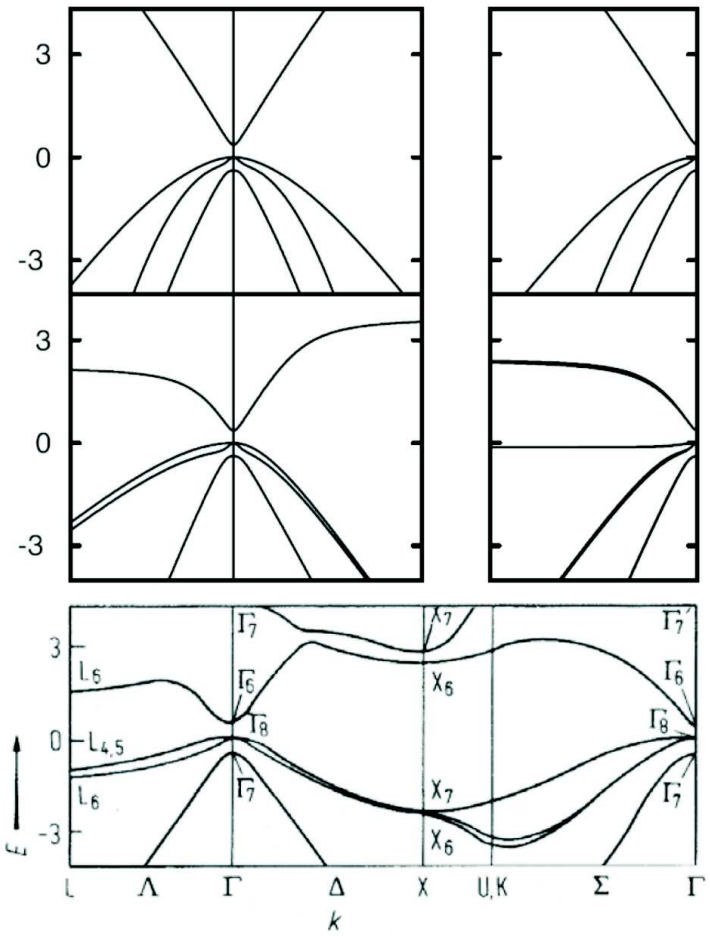

Figure 3.1: Band structure of InAs calculated in a 8-band model (top), 14-band model (middle) and in non-local pseudopotential model (bottom). After [12] and [15].

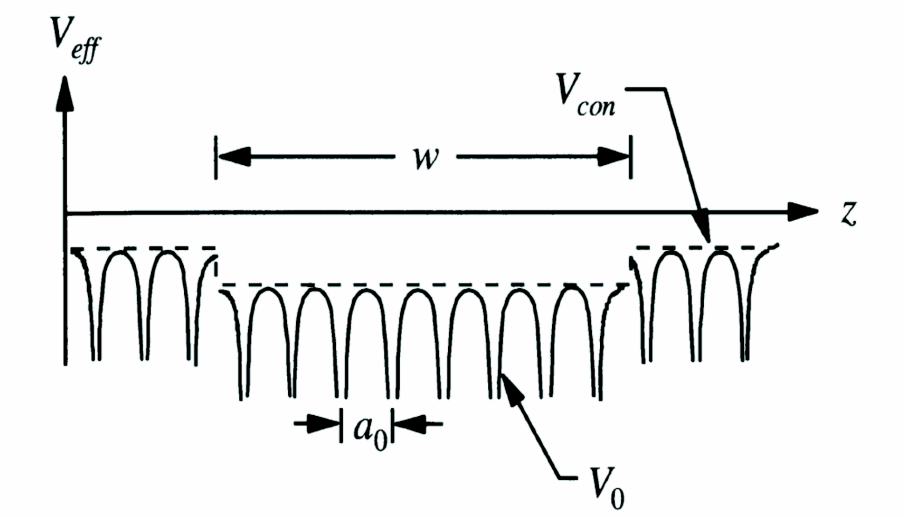

Figure 3.2: Effective potential for a quantum well structure. The picture indicate two length scales on which a variation of the potential occurs: the one is characterized by the quantum well width w, and the other one is characterized by the bulk lattice constant a_0.

total potential is: $\bar{V} = V_0 + V_{conf}$, where $V_{conf} = V_{conf}(z)$, a potential which varies only along the growth direction z, is schematically presented in Fig. 3.2. We assume that the potential V_{conf} is sufficiently small, in comparison to V_0, and varies only slightly within a unit cell, so that the eigenestates of the heterostructure can still be approximated by a linear superposition of bulk-material eigenstates:

$$|\phi_L^{QW}>=\sum_{n,\boldsymbol{k}} |n,\boldsymbol{k}><n\boldsymbol{k}|\phi_L^{QW}> . \tag{3.11}$$

Analogously to the bulk-$\boldsymbol{k}\cdot\boldsymbol{p}$ procedure, we write the zone-center superlattice wave functions (denoted with capital letters) in terms of the zone-center bulk wavefunctions:

$$<\boldsymbol{r}|L,\boldsymbol{K}=0>=\sum_{n'} F_{n'}(L,\boldsymbol{r})\ <\boldsymbol{r}|n',0>, \tag{3.12}$$

where $F_{n'}(L,\boldsymbol{r})$ are the expansion coefficients, and the summation runs over all the zone-center bulk states. In this expansion, we assumed that the zone-center bulk wavefunctions are identical for both constituent materials A, B:

$$<\boldsymbol{r}|n0>^A=<\boldsymbol{r}|n0>^B . \tag{3.13}$$

For the superlattice $\boldsymbol{K}\cdot\boldsymbol{p}$ method, the expansion coefficients $F_{n'}(L,\boldsymbol{r})$ are the functions of position, and are referred to as the envelope functions.

Applying the Hamiltonian to the expanded zone-centered superlattice wavefunction

yields:

$$\sum_{n'}\Big[\big(\frac{\hat{p}^2}{2m}F_{n'}(L,\boldsymbol{r})\big)<\boldsymbol{r}|n'0>+\big(\frac{\hat{\boldsymbol{p}}}{m}F_{n'}(L,\boldsymbol{r})\big)\cdot(\boldsymbol{p}<\boldsymbol{r}|n'0>) \\ +F_{n'}(L,\boldsymbol{r})\big(\frac{\hat{p}^2}{2m}+\bar{V}(\boldsymbol{r})\big)<\boldsymbol{r}|n'0>\Big] \\ =E_L(0)\sum_{n'}F_{n'}(L,\boldsymbol{r})<\boldsymbol{r}|n'0>. \tag{3.14}$$

Equation 3.14 simplifies considerably if the envelope functions vary slowly over the spatial scale of an atomic monolayer. Admitting this approximation permits us a simple construction of the eigenvalue equation by operating on it from the left with $\int d^3r <n0|\boldsymbol{r}>$ and averaging over the unit cell. After this, one gets:

$$\sum_{n'}\Big[\big(\frac{\hat{p}^2}{2m}F_{n'}(L,\boldsymbol{r})\delta_{nn'}+\big(\frac{\hat{\boldsymbol{p}}}{m}F_{n'}(L,\boldsymbol{r})\big)\cdot<n0|\hat{\boldsymbol{p}}|n'0>+F_{n'}(L,\boldsymbol{r})<n0|\frac{\hat{p^2}}{2m}+\bar{V}(\boldsymbol{r})|n'0>\Big] \\ =E_L(0)\sum_{n'}F_{n'}(L,\boldsymbol{r})\delta_{nn'}. \tag{3.15}$$

Equation 3.15 can be rewritten as:

$$\sum_{n'}\Big[\big(\frac{\hat{p}^2}{2m}+E_n^{bulk}(\boldsymbol{r})\big)\delta_{nn'}+P_{nn'}^{bulk}(\boldsymbol{r})\cdot\frac{\hat{\boldsymbol{p}}}{m}\Big]F_{n'}(L,\boldsymbol{r})=E_L(0)F_n(L,\boldsymbol{r}),$$

where

$$E_n^{bulk}(\boldsymbol{r})=<n\boldsymbol{0}|\frac{p^2}{2m}+\bar{V}(\boldsymbol{r})|n\boldsymbol{0}>, \tag{3.16}$$

$$P_{nn'}^{bulk}(\boldsymbol{r})=<n\boldsymbol{0}|\boldsymbol{p}|n'\boldsymbol{0}>. \tag{3.17}$$

Similarly to the bulk $\boldsymbol{k}\cdot\boldsymbol{p}$ theory, in heterostructure adapted $\boldsymbol{K}\cdot\boldsymbol{p}$ method, the bulk wavefunctions do not appear explicitly in Eq. 3.16. They are replaced by superlattice energies and envelope functions. The separation of the bulk and superlattice spatial scales, using envelope functions, reduces the problem to that of a continuum system with modulated bulk band edges (with an additional term that mixes the different bulk bands). These equations are solved at the band-center of the superlattice ($\boldsymbol{K}=\boldsymbol{0}$) to yield the band-center envelope functions and superlattice energies.

Once a restricted basis of the band-center superlattice states is chosen [through determining $F_n(L,\boldsymbol{r})$], it becomes a new basis, similarly to the bulk basis case. The superlattice states at finite wavevector can then be expressed as a sum of coefficients multiplying the elements of the band-center superlattice states, as in Ref. [13]:

$$<\boldsymbol{r}|L\boldsymbol{K}>=e^{i\boldsymbol{K}\cdot\boldsymbol{r}}\sum_{N'}c_{LN'}(\boldsymbol{K})<\boldsymbol{r}|N'\boldsymbol{0}>, \tag{3.18}$$

where the $c_{LN'}(\boldsymbol{K})$ are the expansion coefficients. Substituting this again into the eigenvalue

equation yields:

$$\sum_{N'} c_{LN'}(\boldsymbol{K})\Big[\big(\frac{\hat{p}^2}{2m}e^{i\boldsymbol{K}\cdot\boldsymbol{r}}\big) <\boldsymbol{r}|N'0> +\big(\frac{p}{m}e^{i\boldsymbol{K}\cdot\boldsymbol{r}}\big)\cdot\big(\hat{\boldsymbol{p}} <\boldsymbol{r}|N'0>\big) \\ +e^{i\boldsymbol{K}\cdot\boldsymbol{r}}\big(\frac{\hat{p}^2}{2m}+\bar{V}(\boldsymbol{r})\big) <\boldsymbol{r}|N'0>\Big] \\ = E_L(\boldsymbol{K})e^{i\boldsymbol{K}\cdot\boldsymbol{r}}\sum_{N'} c_{LN'}(\boldsymbol{K}) <\boldsymbol{r}|N'0> . \tag{3.19}$$

Acting on Eq. 3.19 with $\int d^3r e^{i\boldsymbol{K}\cdot\boldsymbol{r}} <N0|\boldsymbol{r}>$ results in:

$$\sum_{N'} c_{LN'}(\boldsymbol{K})\Big[\Big(-\frac{\hbar^2K^2}{2m}+E_N(0)\Big)\delta_{NN'}+\frac{\hbar\boldsymbol{K}}{m}\cdot\boldsymbol{P}_{NN'}(0)\Big] = E_L(\boldsymbol{K})c_{LN}(\boldsymbol{K}), \tag{3.20}$$

where

$$E_L(0) = <N\boldsymbol{0}|\frac{p^2}{2m}+\bar{V}(\boldsymbol{r})|N\boldsymbol{0}>, \tag{3.21}$$

$$P_{NN'}(\boldsymbol{0}) =<N\boldsymbol{0}|\boldsymbol{p}|N\boldsymbol{0}> \tag{3.22}$$

are the energy levels and momentum matrix elements coupling the band-center superlattice states.

The term in brackets in Eq. 3.20 represents the superlattice $\boldsymbol{K}\cdot\boldsymbol{p}$ matrix. It can be diagonalized at any point in the Brillouin zone and the set of eigenvalues comprise the superlattice energy levels. The eigenvectors of the $\boldsymbol{K}\cdot\boldsymbol{p}$ matrix are the coefficients that rotate the zone center states into the finite $\boldsymbol{K}$ states. Coefficients $c_{LN}(\boldsymbol{K})$ are called envelope functions. Further simplifications are obtained if we restrict ourselves to the conduction band (in applications, we are mostly interested in the *electron* transport), which is a single band with spin-degeneracy.

Multiplying again Eq. 3.20 with $<N0|$, taking equation for $N' := N$, using the fact that $\boldsymbol{P}_{NN}(0) = 0$ (as energy of the band reaches its minimum in the center, see Ref. [3]), gives:

$$c_{LN}(\boldsymbol{K})\Big[-\frac{\hbar^2K^2}{2m_c(\boldsymbol{r})}+E_N(0)+\frac{\hbar\boldsymbol{K}}{m_c}\cdot\boldsymbol{P}_{NN}(0)\Big] = E_L(\boldsymbol{K})c_{LN}(\boldsymbol{K}) \\ \Downarrow \\ c_{LN}(\boldsymbol{K})\Big[-\frac{\hbar^2K^2}{2m_c(\boldsymbol{r}))}+E_N(0)\Big] = E_L(\boldsymbol{K})c_{LN}(\boldsymbol{K}). \tag{3.23}$$

To turn from the momentum space to the coordinate space, we apply to Eq. 3.23 the Fourier transform. In real space, the eigenfuntions $c_{LN}(\boldsymbol{r})$ can be represented as products:

$$c_{LN}(\boldsymbol{r}) = f_\nu(z)\cdot U_N(\boldsymbol{r}_\perp), \tag{3.24}$$

where $L\to\nu$, and $\boldsymbol{r}_\perp$ is vector, which lies in the plane of the heterostructure. Using the fact that $\bar{V} = V_0 + V_{conf}$, where V_{conf} is a slowly varying potential in the scale of the layer thickness, we can write that $E_N(\boldsymbol{r}) \approx E_c^{bulk} + V_{conf}(z)$. Hence, for the z-dependent part of envelope function in the conduction band we get:

$$\Big[-\frac{d}{dz}\frac{\hbar^2}{2m_c(z)}\frac{d}{dz}+E_c^{bulk}(z)+V_{conf}(z)\Big]f_\nu(z) = E_\nu f_\nu(z). \tag{3.25}$$

In SL, the confinement mass $m_c(z)$ replaces the effective electron mass of the conduction band the crystal m_c in z-direction. Since the effective mass in the z-direction of a quantum-well heterostructure depends on space (through V_{conf} and m_c of constituent materials), we have to symmetrize the second derivative to assure that the Hamiltonian is Hermitian. Function $U_N(\boldsymbol{r}_\perp)$ obeys the equation:

$$-\frac{\hbar^2}{2m_c}\nabla_\perp^2 U_N(\boldsymbol{r}_\perp) = E_\perp U_N(\boldsymbol{r}_\perp). \tag{3.26}$$

The total energy of the electrons in the superlattice band has a contribution from the quantum confinement V_{conf} and the free motion in the $x-y$ plane $E_\perp$.

The presented schemes, based on the EFA, are expected to work well for superlattices comprising of thick layers, in which the artificial super-period d is much larger than the period of the crystal lattice a_0. The additional assumtions laying behind the these derivations are that compounds show structural and chemical similarity, individual layers can be viewed as macroscopic crystals, and that differences between rapidly varying parts of the corresponding bulk Bloch functions can be ignored. By removing the rapidly varying part of the wave-function from the problem, the solution of the Schrodinger equation is made independent of microscopic aspects controling the alignment of the two bulk band structures. Although the model Hamiltonians based on the EFA have been used very successfully to interpret experiments on thick-layered systems, they cannot be used easily to probe the physical mechanisms underlying the processes of confinement and electron localization at interfaces. In superlattice systems comprising ultra-thin (~ 20) layers, coupling occurs between remote bulk bands and so the dispersion of these bands seems to be of importance.

3.3. Minibands - an extension of the Kronig-Penney model

The first quantum mechanics analysis of periodic wells and barriers system was proposed by Kronig and Penney, who took a rectangular potential as an approximation of the crystal potential for bulk matter investigations. The original Kronig-Penney (KP) model describes an electron in a one-dimensional periodic potential of quantum wells, and has an analytical solution (see [14]). The wavefunctions of a single-electron Hamiltonian, for both, region of well and region of barrier of height V_0 in that model, obey the equations:

$$\frac{d^2\psi}{dz^2} + \frac{2m}{\hbar^2}(E - V_0)\psi = 0 \qquad (well) \tag{3.27}$$

$$\frac{d^2\psi}{dz^2} + \frac{2m}{\hbar^2}E\psi = 0 \qquad (barrier) \tag{3.28}$$

$$\tag{3.29}$$

Solutions to the above equations have the form of plane waves:

$$\psi_{well} = Aexp(ik_\beta z) + Bexp(-ik_\beta z), \qquad k_\beta = \sqrt{\frac{2m(E-V_0)}{\hbar^2}} \tag{3.30}$$

$$\psi_{barrier} = Cexp(ik_\alpha z) + Dexp(-ik_\alpha z), \qquad k_\alpha = \sqrt{\frac{2mE}{\hbar^2}} \tag{3.31}$$

where A, B, C, D, are complex coefficients obtained from boundary conditions (both ψ and $d\psi/dz$ are continuous functions of z).

A three dimensional picture explaining the formation of minibands in SL can be obtained from the application of Bloch theorem and Kronig -Penney model to the description of states in the growth direction. The crystal translational symmetry in the in-plane directions (spanned by K_x and K_y) is not modified, so the bulk wavevector in the in-plane direction remain a good quantum number (i.e., k_x is equivalent to K_x and k_y is equivalent to K_y). For the sake of simplicity, the superlattice wavevector K_z will be denoted as q, hence $\boldsymbol{K} = [q, \boldsymbol{k}]$, where $\boldsymbol{k} = [k_x, k_y]$. The periodicity of the superlattice structure along z direction implies that the eigenstates of the Hamiltonian can be written as a product of plane waves and Bloch states $\varphi = \sum_\nu e^{i(k_x r_x + k_y r_y)}/(2\pi) \cdot \varphi_q^\nu$, where $q \in [-\frac{\pi}{d}, \frac{\pi}{d}]$ denotes the Bloch vector, and the Bloch function $\varphi_q^\nu = e^{iqz} f_\nu(z)$. The envelope functions $f_\nu(z)$ obey the eigenvalue equation:

$$\Big(E_c(z) - \frac{\partial}{\partial z}\frac{\hbar^2}{2m_c(z)}\frac{\partial}{\partial z} + \frac{\hbar^2 \boldsymbol{k}^2}{2m_c(z)}\Big) f_\nu(z) = E_\nu f_\nu(z). \tag{3.32}$$

Although the Hamiltonian is not exactly separable into a z- and $\boldsymbol{r}$-dependent part [z-dependent effective mass affects $\boldsymbol{k}$-dependence, which describes the behavior in (x, y) plane], we treat the problem as if it was the case. As material composition are constant within a region of well/barrier $z_j < z < z_{j+1}$ (in other words, $E_{c,j}, m_{c,j}, V_{conf} = const$ for $z_j < z < z_{j+1}$), hence, the envelope function can be written as $f_c(z) = A_j e^{ik_j(E)(z-z_j)} + B_j e^{-ik_j(E)(z-z_j)}$.

Then the continuity rules, derived for case of abrupt junction of two materials with dissimilar one-electron periodic potentials (we impose the conservation of current and "local" matching of envelope functions at interfaces), gives the following boundary conditions (after [5]):

$$\begin{aligned} f_c(\boldsymbol{r})_{z\to z_{j+1}+0^-} &= f_c(\boldsymbol{r})_{z\to z_{j+1}+0^+}, \\ \frac{1}{m_{c,j}}\frac{\partial f_c(\boldsymbol{r})}{\partial z}_{z\to z_{j+1}+0^-} &= \frac{1}{m_{c,j+1}}\frac{\partial f_c(\boldsymbol{r})}{\partial z}_{z\to z_{j+1}+0^+}, \end{aligned} \tag{3.33}$$

where $m_{c,j}$ is the effective mass in region $z_j < z < z_{j+1}$. Substituting f_c in Eq. 3.33, we get a set of ordinary linear equations (for detailed derivation see Appendix A) in the form:

$$\begin{aligned} \begin{pmatrix} A_{j+1} \\ B_{j+1} \end{pmatrix} &= \mathcal{M}_j(E) \begin{pmatrix} A_j \\ B_j \end{pmatrix} \\ &= \frac{1}{2}\begin{pmatrix} (1+\frac{k_j m_{c,j+1}}{k_{j+1} m_{c,j}})e^{ik_j(z_{j+1}-z_j)} & (1-\frac{k_j m_{c,j+1}}{k_{j+1} m_{c,j}})e^{-ik_j(z_{j+1}-z_j)} \\ (1-\frac{k_j m_{c,j+1}}{k_{j+1} m_{c,j}})e^{ik_j(z_{j+1}-z_j)} & (1+\frac{k_j m_{c,j+1}}{k_{j+1} m_{c,j}})e^{-ik_j(z_{j+1}-z_j)} \end{pmatrix} \begin{pmatrix} A_j \\ B_j \end{pmatrix}. \end{aligned} \tag{3.34}$$

The Bloch condition $\varphi(z+d) = e^{iqd}\varphi(z)$ implies that:

$$\begin{pmatrix} A_{n+1} \\ B_{n+1} \end{pmatrix} = \mathcal{M}_j(E)^n \begin{pmatrix} A_1 \\ B_1 \end{pmatrix} = e^{inqd} \begin{pmatrix} A_1 \\ B_1 \end{pmatrix}. \tag{3.35}$$

Note that this approach can be straightforwardly extended to more complicated superlattices, in which the single period consist of M different regions with a constant material composition. It is particularily useful for modeling QCL structure, where each period usually consists of 3 quantum wells of active region and dozen of quantum wells of collecting/injecting region. For each q value, we determine $E^\nu(q)$ numerically, by looking for the zeroes of the determinant of the matrix product. Once the $E^\nu(q)$ are determined, we can also obtain A_1 and B_1, and after that the Bloch functions φ_q^ν. For a given value of q Eq. 3.35 has solutions only for certain values of E: this defines the miniband structure $E^\nu(q)$.

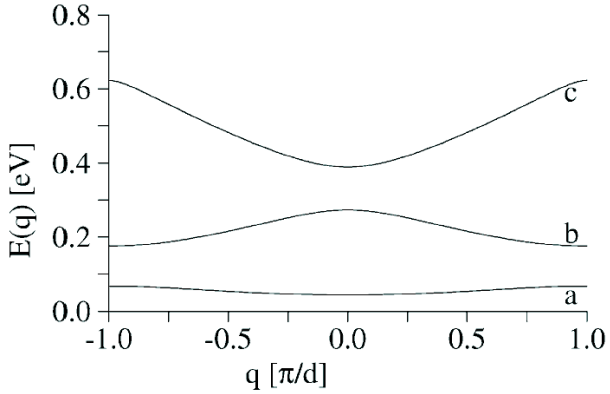

Figure 3.3: Calculations of miniband structure basing on transfer matrix method, for the $GaAs - Al_{0.3}Ga_{0.7}As$ superlattice, with the well width 6.5 nm and the barrier width 2.5 nm. After [4].

The minibands are much more narrow than those in bulk material. Hence, it is reasonable to address to a given miniband ν the following quantities:
center of miniband: $E^\nu = d/(2\pi)\int_{-\pi/d}^{\pi/d} dq E^\nu(q)$,
miniband width: $\Delta^\nu = Max_q\{E^\nu(q)\} - Min_q\{E^\nu(q)\}$.

The width of the miniband increases with its number ν, which corresponds to the increase of transparency of the barrier for the electron. As $E^\nu(q) \in (-\pi/d, \pi/d)$ and $E^\nu(q) = E^\nu(-q)$ due to the Krammers degeneracy (assumed at the beginning), miniband energy $E^\nu(q)$, as a periodic even function, can be expanded into a cosine series:

$$E^\nu(q) = E^\nu + \sum_{h=1}^{\infty} 2T_h^\nu \cos(hdq). \tag{3.36}$$

Typically, the terms T_h^ν for $h \geq 2$ are an order or two orders of magnitude smaller than T_1^ν, which demonstrates that the band structure is essentially of cosine shape [from definition $\Delta^\nu \approx 4|T_1^\nu|$ and dispersion $E^\nu(q) \approx E^\nu + 2T_1^\nu \cos(dq)$]. This result can be connected to a standard tight-binding model, where T_1^ν is interpreted as the nearest-neighbor-well coupling.

Taking into account all 3 dimensions and a parabolic approximation (first order perturbation theory for the bulk states), the energy can be written as:

$$E^\nu(q, k_x, k_y) \approx E^\nu(q, \mathbf{0}) + \frac{\hbar^2 \boldsymbol{k}^2}{2m_{well}}. \tag{3.37}$$

Expressing the superlattice Hamiltonian in terms of creation ($a_q^{\nu\dagger}$) and annihilation (a_q^ν) operators for electrons in the band ν and Bloch wavevector q, we get:

$$\hat{H}_{SL} = \sum_\nu \int_{-\pi/d}^{\pi/d} dq \int d^2k \; [E^\nu(q) + E_k] \; a_q^{\nu\dagger} a_q^\nu, \tag{3.38}$$

which contains just diagonal terms, because Bloch states are eigenstates of the unperturbed superlattice. As we indicated at the beginning of the chapter, the Bloch functions, due to their spatial extension over the whole structure, cannot be directly used to analyze the Hamiltonian with an external field. To handle this problem, we have to introduce different functions, the so-called Wannier functions (see Ref. [8]).

3.4. Wannier functions

A disadvantage of the use of Bloch functions is that they, by definition, are delocalized over the whole superlattice structure (of infinite length), which may cause difficulties when finite size effects have to be considered. It is important to note that the widths of the low-lying minibands are extremely small, similar to flat bands descibing classically bounded motion (see calculations of band widths in Ref. [11]). Therefore, it is useful to take different orthonormal set of basis states - better localized and almost nondispersive (i.e. quasistationary). A convenient choice is to use Wannier functions, associated with miniband ν:

$$\Psi^{\nu}(z-nd) = \sqrt{\frac{d}{2\pi}} \int_{-\pi/d}^{\pi/d} dq e^{-inqd} \varphi_q^{\nu}(z), \tag{3.39}$$

which are constructed from the Bloch functions $\varphi_q^{\nu} = e^{iqz} f_{\nu}(z)$, with the normalization condition $\int dz [\varphi_{q'}^{\nu'}(z)]^* \varphi_q^{\nu}(z) = \delta_{\nu\nu'}\delta(q-q')$. The Wannier functions defined in this way are not unique with respect to complex phase, as the phase choice of the constituent Bloch functions φ_q^{ν} is arbitrary for each value of q (Bloch function φ multiplied by factor $e^{i\theta}$ is still Bloch function of the same state). Ideally, we would like the Wannier functions to be as spatially localized as possible, to reduce the interaction matrix elements between Wannier functions from different periods (off-diagonal coupling between levels in different periods), and hence to simplify calculations. With a proper phase choice localization can be improved (see the discussion of arbitrary phase choice of $\varphi_q^{\nu}(z)$ in the expansion 3.39 in Ref. [7]).

The Wannier functions exhibit the ortonormality condition:

$$\int dz \Psi^{\nu}(z-nd)\Psi^{\mu}(z-md) = \delta_{n,m}\delta_{\nu,\mu}, \tag{3.40}$$

but this is not strictly fulfilled when we consider in Eq. 3.32 energy dependent (band dependent) effective mass. In such a case, the Bloch functions of different bands diagonalize different energy-dependent Hamiltonian. In principle, one of the strategies to treat this problem is to reconstruct the full wave functions from envelope functions, considering also admixtures from different bands. In practice, however, we neglect this discrepancy. As the Wannier functions are linear combinations of the Bloch functions with different energies, they do not represent stationary states (they are not eigenstates of the Hamiltonian). Therefore, it is difficult to obtain a direct physical interpretation in the energy domain. For instance, there is no one-to-one correspondence between an optical transition in the structure and a transition between a pair of Wannier functions, that is their main disadvantage.

The Wannier states time-evolution can be found by introducing the formalism of second quantization. Let $a_q^{\nu\dagger}$ and a_q^{ν} be creation and annihilation operators for electrons in the Wannier state. The annihilation operators associated with the Wannier functions $\Psi^{\nu}(z-nd)$ in the momentum space are defined according to the relation: $a_q^{\nu} = \sqrt{\frac{d}{2\pi}} \sum_n e^{-iqnd} a_n^{\nu}$. The Hamiltonian for the superlattice has the form:

$$\hat{H}_{SL} = \sum_{\nu} \int_{-\pi/d}^{\pi/d} E^{\nu}(q) a_q^{\nu\dagger} a_q^{\nu}. \tag{3.41}$$

Substituting Eq. 3.36 into Eq. 3.41 and passing from the Bloch basis to the Wannier basis (for a full derivation see Appendix B), we get:

$$\hat{H}_{SL} = \sum_{n,\nu} \Big[E^{\nu} a_n^{\nu\dagger} a_n^{\nu} + \sum_{h=1}^{\infty} T_h^{\nu} (a_{n+h}^{\nu\dagger} a_n^{\nu} + a_{n-h}^{\nu\dagger} a_n^{\nu}) \Big]. \tag{3.42}$$

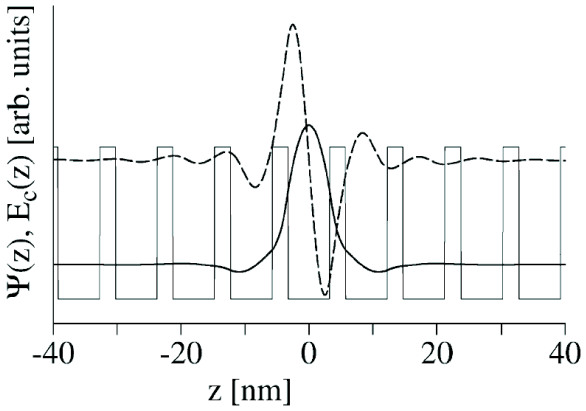

Figure 3.4: Wannier functions for the same superlattice as in Fig. 3.3. The solid and dashed curves represent $\Psi^a(z)$ and $\Psi^b(z)$, respectively. The thin line indicates the conduction band edge profile. From the plot it is seen that the Wannier functions are well localized inside a well. After [4]

Neglecting terms with $h > 1$ (higher terms are much smaller as compared to T_1^ν), and bearing in mind that:

$$\frac{da_n^\nu(t)}{dt} = \frac{i}{\hbar}[a_n^\nu(t), \hat{H}_{SL}],$$

we arrive at the time evolution equation for annihilation operators in a form:

$$i\hbar\frac{d}{dt}a_n^\nu(t) = E^\nu a_n^\nu(t) + T_1^\nu[a_{n+1}^\nu(t) + a_{n-1}^\nu(t)]. \tag{3.43}$$

Under the initial condition, $a_n^\nu(t=0) = \delta_{n,0}a_0^\nu$, the solution to Eq. 3.43 is (for a full derivation see Appendix C):

$$a_n^\nu(t) = i^{-n}J_n(\frac{2T_1^\nu}{\hbar}t)e^{-iE^\nu t/\hbar}a_0^\nu, \tag{3.44}$$

where $J_n(x)$ is the Bessel function of the first kind.

Applying the electric field F to the superlattice requires adding to the Hamiltonian an external potential $\phi(z) = -Fz$. The total Hamiltonian [taking into account (x,y)-dependence in the parabolic band approximation (Eq. 3.37)] can be split into 3 parts, $\hat{H} = \hat{H}_0 + \hat{H}_1 + \hat{H}_2$:

$$\hat{H}_0 = \sum_{n,\nu}\int d^2k(E^\nu + E_k - eFR_0^{\nu\nu} - eFdn)a_n^{\nu\dagger}(\boldsymbol{k})a_n^\nu(\boldsymbol{k}), \tag{3.45}$$

$$\hat{H}_1 = \sum_{n,\nu,\mu}\sum_{h=1}^{\infty}\int d^2k\{T_h^\nu[a_{n+h}^{\nu\dagger}(\boldsymbol{k})a_n^\nu(\boldsymbol{k}) + a_n^{\nu\dagger}(\boldsymbol{k})a_{n+h}^\nu(\boldsymbol{k})]\delta_{\mu,\nu} - eFR_h^{\mu\nu}[a_{n+h}^{\mu\dagger}(\boldsymbol{k})a_n^\nu(\boldsymbol{k}) + a_n^{\nu\dagger}(\boldsymbol{k})a_{n+h}^\mu(\boldsymbol{k})]\}, \tag{3.46}$$

$$\hat{H}_2 = \sum_{\substack{n,\nu,\mu \\ \nu\neq\mu}}\int d^2k(-eFR_0^{\mu\nu})a_n^{\mu\dagger}(\boldsymbol{k})a_n^\nu(\boldsymbol{k}), \tag{3.47}$$

where $R_h^{\mu\nu} = \int dz\Psi^\mu(z-hd)z\Psi^\nu(z)$ (see Ref. [4]). If the superlattice exhibits the inversion symmetry (the functions Ψ^μ and Ψ^ν are even) then the $R_h^{\nu\nu}$ vanish for $h > 0$. The term $\hat{H}_0$

denotes the energy of superlattice states in the absence of any coupling to the other bands and wells. $\hat{H}_1$ corresponds to the coupling between different wells. Finally, $\hat{H}_2$ describes the field-induced mixing of levels inside a given well.

3.5. Applying of an external electric field - Wannier-Stark states

If an electric field F is applied to the superlattice structure, the Hamiltonian acquires an additional scalar potential $\phi(z) = -eFz$, which breaks the translational symmetry of the field-free Hamiltonian in z-direction. According to the Wannier's theorem, if $\Phi_0(z)$ is an eigenfunction of the Hamiltonian with energy E_0, then the set of states $\Phi_j(z) = \Phi_0(z - jd)$ are also its eigenfunctions, with energies $E_j = E_0 - jeFd$. These states are equally spaced both in energy and real space and form the so-called Wannier-Stark ladder (see Ref. [16] and Ref. [18]).

For a superlattice it means that within the single band approximation, if the ν'th miniband with the mean energy E^ν and wavefunction $\Phi^\nu(z)$ is a solution of the field-free Hamiltonian $\hat{H}_{SL}$ (Eq. 3.41), then in an external field, the Wannier-Stark states diagonalize the Hamiltonian with the field, and a ladder with the quantized energies is formed:

$$E_j^\nu = E^\nu - jeFd, \tag{3.48}$$

where E^ν is the mean energy of the ν-th miniband. An analytical solution for eigenstates of $\hat{H}_{SL} - eFz$ reads (after [9]):

$$|\Phi_j^\nu >= \sqrt{\frac{d}{2\pi}} \int_{-\pi/d}^{\pi/d} dq exp\Big\{\frac{i}{eF}\int_0^q dq'[E_j^\nu - E^\nu(q')]\Big\}|\varphi_q^\nu > . \tag{3.49}$$

For a cosine-shaped band $E_q^\nu = E^\nu + 2T_1^\nu cos(qd)$, the Wannier-Stark states given by Eq. 3.49 can be expanded in terms of Wannier states $\Psi^\nu(z - nd) = |\Psi_n^\nu >$ as:

$$|\Phi_j^\nu >= \sum_{n=-\infty}^{\infty} J_{n-j}\Big(\frac{2T_1^\nu}{eFd}\Big)|\Psi_n^\nu > . \tag{3.50}$$

A detailed derivation is presented in Appendix D. An important property of these functions is that their localization gets stronger with increasing the electric field. The process, which is neglected in the single band approximation and which is a consequence of coupling between the minibands, is the Zener tunneling (see Ref. [20]). As the band gap decreases with increasing band index, and the tunneling rate increases with decreasing band gap, electrons asymmetrically tend to tunnel to higher minibands. Hence, the band population depletes with time. (It has been proven that beyond the one-band approximation the spectrum of the Hamiltonian is continuous, see Ref. [21]). Thus, the discrete spectrum from Eq. 3.48 (ladder) can refer only to resonances, and should be corrected as:

$$E_j^\nu = E^\nu - jeFd - i\frac{\Gamma_\nu}{2}. \tag{3.51}$$

The eigenstates corresponding to these complex energies are metastable states with the lifetime given by $\tau = \hbar/\Gamma_\nu$, where Γ_ν is a tunneling rate. Clear physical interpretation is the main advantage of usage Wannier-Stark description over Wannier functions description.

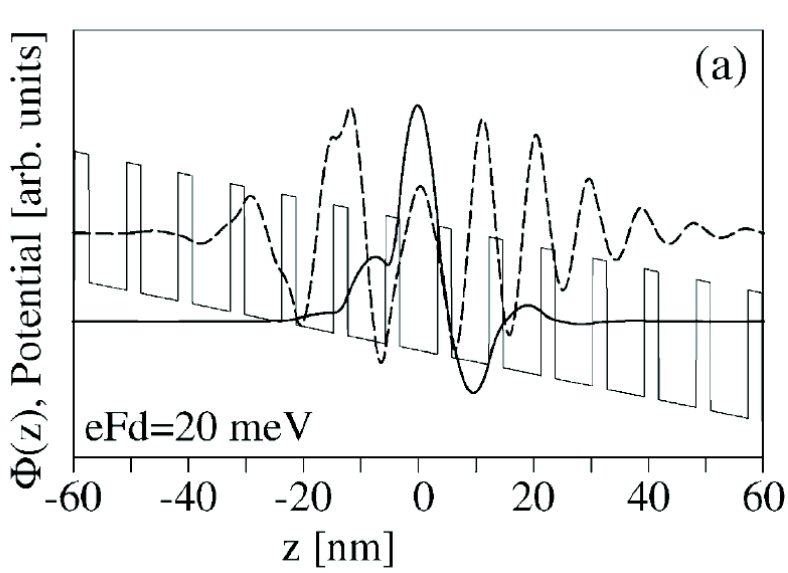

Figure 3.5: Wannier-Stark states for the same superlattice as in Fig. 3.3, obtained from Eq. 3.49. As before, the solid and dashed curves represent $\Phi^a(z)$ and $\Phi^b(z)$, respectively. The thin line indicates the conduction band edge profile. After [4]

.

Chapter 4

Summary

This report gives a short introduction to the quantum cascade lasers and describes basic theoretical analysis of superlattices, which are the source for further more detailed investigations. It does not cover many important issues of band description, like incorporation of superlattice interface states between constituent materials. Moreover, from the practical point of view, the description and calculation of current through the structure (including phonon-assisted tunneling or radiative transitions) are of even bigger interest than the band structure itself. Those subjects, however, refere to much more advanced concepts of the quantum electron transport and they are covered by the other reviews, where the presented here knowledge is required as a background. Therefore, a detailed explanation and deep reasoning given here is a useful reference for unexperienced reader. It was difficult to give detailed explanations of fundamental concepts and not exceed the frame of the short report, as much as difficult is summarizing the 40 years of work done all over the world on semicontuctor superlattice, both theoretical and experimental, on 40 pages, without referring to more advanced concepts. For further studies, it is recommended to read, for example, Ref. [4], [19] and [22].

Appendix A

Here, we derive the matrix $M_j(E)$, which determins coefficients for the envelope function. The envelope function in the region of well/barrier $z_j < z < z_{j+1}$ is written as $f_c(z) = A_j e^{ik_j(E)(z-z_j)} + B_j e^{-ik_j(E)(z-z_j)}$. Then the boundary conditions read:

$$\begin{aligned} (a) \qquad & f_c(\boldsymbol{r})_{z\to z_{j+1}+0^-} = f_c(\boldsymbol{r})_{z\to z_{j+1}+0^+}, \\ (b) \qquad & \frac{1}{m_{c,j}}\frac{\partial f_c(\boldsymbol{r})}{\partial z}_{z\to z_{j+1}+0^-} = \frac{1}{m_{c,j+1}}\frac{\partial f_c(\boldsymbol{r})}{\partial z}_{z\to z_{j+1}+0^+}. \end{aligned} \tag{A.1}$$

Substituting the formula for f_c into Eq. A.1 gives:

$$\begin{aligned} A_j e^{ik_j(z_{j+1}-z_j)} + B_j e^{-ik_j(z_{j+1}-z_j)} &= A_{j+1}e^{ik_{j+1}(z_{j+1}-z_j)} + A_{j+1}e^{ik_{j+1}(z_{j+1}-z_j)}, \\ \frac{1}{m_{c,j}}\Big[ik_j A_j e^{ik_j(z_{j+1}-z_j)} - ik_j B_j e^{ik_j(z_{j+1}-z_j)}\Big] &= \\ = \frac{1}{m_{c,j+1}}\Big[ik_{j+1}A_{j+1}e^{ik_{j+1}(z_{j+1}-z_j)} &- ik_{j+1}B_{j+1}e^{ik_{j+1}(z_{j+1}-z_j)}\Big]. \end{aligned} \tag{A.2}$$

Eq. A.2 can be rewritten in the matrix form as follows:

$$\begin{aligned} &\begin{pmatrix} e^{ik_j(z_{j+1}-zj)} & e^{-ik_j(z_{j+1}-zj)} \\ \frac{ik_j}{m_{c,j}}e^{ik_j(z_{j+1}-zj)} & -\frac{ik_j}{m_{c,j}}e^{-ik_j(z_{j+1}-zj)} \end{pmatrix} \cdot \begin{pmatrix} A_j \\ B_j \end{pmatrix} = \\ &\qquad \begin{pmatrix} e^{ik_{j+1}(z_{j+1}-zj)} & e^{-ik_{j+1}(z_{j+1}-zj)} \\ \frac{ik_{j+1}}{m_{c,j+1}}e^{ik_{j+1}(z_{j+1}-zj)} & -\frac{ik_{j+1}}{m_{c,j+1}}e^{-ik_{j+1}(z_{j+1}-zj)} \end{pmatrix} \cdot \begin{pmatrix} A_{j+1} \\ B_{j+1} \end{pmatrix}, \end{aligned} \tag{A.3}$$

or in a compact form:

$$\mathcal{X} \cdot \begin{pmatrix} A_j \\ B_j \end{pmatrix} = \mathcal{Y} \begin{pmatrix} A_{j+1} \\ B_{j+1} \end{pmatrix}. \tag{A.4}$$

Further, we can solve this equation with respect to A_{j+1} and B_{j+1}, introducing the inverse matrix $\mathcal{Y}^{-1}$:

$$\begin{pmatrix} A_{j+1} \\ B_{j+1} \end{pmatrix} = \mathcal{Y}^{-1} \cdot \mathcal{X} \begin{pmatrix} A_j \\ B_j \end{pmatrix}, \tag{A.5}$$

where

$$\mathcal{Y}^{-1} = \frac{im_{c,j+1}}{2k_{j+1}} \begin{pmatrix} A_j \\ B_j \end{pmatrix} = \begin{pmatrix} -\frac{ik_{j+1}}{m_{c,j+1}}e^{-ik_{j+1}(z_{j+1}-zj)} & -e^{ik_{j+1}(z_{j+1}-zj)} \\ -\frac{ik_{j+1}}{m_{c,j+1}}e^{ik_{j+1}(z_{j+1}-zj)} & e^{ik_{j+1}(z_{j+1}-zj)} \end{pmatrix}.$$

After multiplying the matrixes, we arrive at the final expresion:

$$\begin{aligned}\begin{pmatrix} A_{j+1} \\ B_{j+1} \end{pmatrix} &= \mathcal{M}_j(E) \begin{pmatrix} A_j \\ B_j \end{pmatrix} \\ &= \frac{1}{2} \begin{pmatrix} (1+\frac{k_j m_{c,j+1}}{k_{j+1} m_{c,j}}) e^{ik_j(z_{j+1}-zj)} & (1-\frac{k_j m_{c,j+1}}{k_{j+1} m_{c,j}}) e^{-ik_j(z_{j+1}-zj)} \\ (1-\frac{k_j m_{c,j+1}}{k_{j+1} m_{c,j}}) e^{ik_j(z_{j+1}-zj)} & (1+\frac{k_j m_{c,j+1}}{k_{j+1} m_{c,j}}) e^{-ik_j(z_{j+1}-zj)} \end{pmatrix} \begin{pmatrix} A_j \\ B_j \end{pmatrix},\end{aligned} \tag{A.6}$$

that is we want to prove.

Appendix B

Here, we show how to obtain the formula of Hamiltonian in terms of the creation operator, $a_q^{\nu\dagger}$, (The Hamiltonian in terms of anihilation operators, a_q^{ν}, can be obtained analogously).

For an electron in the Bloch state of the ν'th band the Hamiltonian has the form:

$$\hat{H}_{SL} = \sum_{\nu} \int_{-\pi/d}^{\pi/d} dq E^{\nu}(q) a_q^{\nu\dagger} a_q^{\nu}. \tag{B.1}$$

Within the second quantisation scheme, the anihilation operators a_q^{ν} associated with Bloch functions, and anihilation operators a_n^{ν} associated with Wannier states, satisfy the relation:

$$a_q^{\nu} = \sqrt{\frac{d}{2\pi}} \sum_n e^{-iqnd} a_n^{\nu}. \tag{B.2}$$

Substituting Eq. B.2 into Eq. B.1, and using the orthonormality condition:

$$\frac{d}{2\pi} \int_{-\pi/d}^{\pi/2} dq \sum_m \sum_n e^{-iqnd} e^{iqmd} = \delta_{mn}, \tag{B.3}$$

and along with the relation $cos(hdq) = \frac{1}{2}(exp(ihdq) + exp(-ihdq))$, we go through the following steps:

$$\hat{H}_{SL} = \sum_{nu} \int_{-\pi/d}^{\pi/d} dq \Big(E^{\nu} + \sum_h T_h^{\nu} (e^{ihdq} + e^{-ihdq}) \Big) \cdot \frac{d}{2\pi} \sum_n e^{iqnd} a_n^{\nu\dagger} \sum_m e^{-iqmd} a_m^{\nu} =$$

$$\sum_{nu} E^{\nu} \sum_n a_n^{\nu\dagger} a_n^{\nu} + \sum_{nu} \frac{d}{2\pi} \int_{-\pi/d}^{\pi/d} dq \Big(\sum_h T_h^{\nu} e^{ihdq} + e^{-ihdq} \Big) \cdot \sum_n e^{iqnd} a_n^{\nu\dagger} \sum_m e^{-iqmd} a_m^{\nu}. \tag{B.4}$$

For the sake of simplicity, we denote the first term as FT, and the second one as ST. Using Eq. B.3, $FT = \sum_{\nu,n} E^{\nu} a_n^{\nu\dagger} a_n^{\nu}$.

Let's focus then on the second term:

$$ST = \frac{d}{2\pi} \sum_{nu} \frac{d}{2\pi} \int_{-\pi/d}^{\pi/d} dq \sum_h T_h^{\nu} \left[\sum_n e^{iq(n+h)d} \sum_m e^{-iqmd} a_n^{\nu\dagger} a_m^{\nu} + \sum_n e^{iq(n-h)d} \sum_m e^{-iqmd} a_n^{\nu\dagger} a_m^{\nu} \right] =$$

$$= \sum_{h=1}^{\infty} T_h^{\nu} (a_{n+h}^{\nu\dagger} a_m^{\nu} + a_{n-h}^{\nu\dagger} a_m^{\nu}). \tag{B.5}$$

Thus, the Hamiltonian within the Wannier basis takes the form:

$$\hat{H}_{SL} = \sum_{n,\nu} \Big[E^{\nu} a_n^{\nu\dagger} a_n^{\nu} + \sum_{h=1}^{\infty} T_h^{\nu} (a_{n+h}^{\nu\dagger} a_n^{\nu} + a_{n-h}^{\nu\dagger} a_n^{\nu}) \Big], \tag{B.6}$$

that is we want to prove.

Appendix C

We want to find a solution to the equation:

$$i\hbar\frac{d}{dt}a_n^\nu(t) = E^\nu a_n^\nu(t) + T_1^\nu[a_{n+1}^\nu(t) + a_{n-1}^\nu(t)]. \tag{C.1}$$

As the index ν is irrelevant, it will be omitted in what follows. We look for the solution of Eq. C.1 in the form:

$$a_n = c_n \; exp\Big(\frac{-iEt}{\hbar}\Big), \tag{C.2}$$

where c_n is a new function of t. Substitutung C.2 into C.1 we get the equation for c_n

$$i\hbar\frac{d}{dt}c_n = T_1(c_{n+1} + c_{n-1}), \tag{C.3}$$

which can be rewritten as:

$$2\frac{d}{dt}c_n = -i\frac{2T_1}{\hbar}(c_{n-1} + c_{n+1}). \tag{C.4}$$

This equation is straightforward to solve, bearing in mind the properties of Bessel functions:

$$\begin{gathered}\frac{d}{dt}J_n = J_{n-1} - \frac{n}{t}J_n,\\ \frac{d}{dt}J_n = -J_{n+1} + \frac{n}{t}J_n,\\ \Downarrow\\ 2\frac{d}{dt}J_n = J_{n-1} - J_{n+1}.\end{gathered} \tag{C.5}$$

Multiplying the last formula, in Eq. C.5, by i^{-n}, we come to the expression:

$$\begin{aligned}i^{-n}2\frac{d}{dt}J_n &= i^{-n}(J_{n-1} - J_{n+1}) = i^{-1}[i^{-n-1}J_{n-1} - i^{-n+1}J_{n+1}] = \\ &= i^{-1}[i^{-n-1}J_{n-1} - i^2\cdot i^{-n-1}J_{n+1}] = -i[i^{-(n-1)}J_{n-1} + i^{-(n+1)}J_{n+1}].\end{aligned} \tag{C.6}$$

Comparing the final formula with Eq. C.4, we end up with the solution for coefficients c_n:

$$c_n = i^{-n}J_n\Big(\frac{2T_1}{\hbar}t\Big). \tag{C.7}$$

Taking into account initial condition $a_n(t=0) = a_0$, the solution to Eq. C.1 has the form:

$$a_n = a_0 \; i^{-n}J_n\Big(\frac{2T_1}{\hbar}t\Big)exp\Big(\frac{-iEt}{\hbar}\Big), \tag{C.8}$$

that is we want to prove.

Appendix D

Here, we derive the formula 3.50 in the representation of Wannier states. The starting form of Wannier-Stark states (in the Bloch-states representation $|\varphi_q^\nu>$) is as follows:

$$|\Phi_j^\nu>=\sqrt{\frac{d}{2\pi}}\int_{-\pi/d}^{\pi/d}dq\ exp\Big\{\frac{i}{eF}\int_0^q dq'[E_j^\nu-E^\nu(q')]\Big\}|\varphi_q^\nu>, \tag{D.1}$$

where $E_j^\nu=E^\nu-jeFd$ and E^ν is the mean energy of the ν-th miniband. We restrict ourselves to a cosine-shaped band, where $E_q^\nu=E^\nu+2T_1^\nu cos(qd)$. Hence:

$$E_j^\nu-E^\nu(q')=-jeFd-2T_1^\nu cos(qd). \tag{D.2}$$

Performing the integration, one gets:

$$\int_0^q[E_j^\nu-E^\nu(q')]=-jeFdq-\frac{2T_1^\nu}{d}sin(qd). \tag{D.3}$$

Substituting Eq. D.3 into Eq. D.1 gives:

$$|\Phi_j^\nu>=\sqrt{\frac{d}{2\pi}}\int_{-\pi/d}^{\pi/d}dq\ exp\Big(-ijdq-i\frac{2T_1^\nu}{eFd}sin(qd)\Big)|\varphi_q^\nu>\ . \tag{D.4}$$

Wannier states in the Bloch-states representation have the form (see Eq. 3.39 for comparison):

$$|\Psi_n^\nu>=\sqrt{\frac{d}{2\pi}}\int_{-\pi/d}^{\pi/d}dq\ e^{-inqd}|\varphi_q^\nu>\ . \tag{D.5}$$

Let's consider the Fourier transformation of Bloch functions (which are periodic in real and in reciprocal space):

$$\begin{gathered}\varphi^\nu(z)=\varphi^\nu(z+nd)\quad\wedge\quad\varphi^\nu(q)=\varphi^\nu(q+2\pi/nd)\\ \Downarrow\\ \varphi^\nu(q)=\sum_n\varphi^\nu(z+nd)e^{indq}\\ \Downarrow\\ \varphi_q^\nu=\sum_n\Big\{\frac{d}{2\pi}\int_{-\pi/d}^{\pi/d}dq\ e^{-indq}\varphi_q^\nu\Big\}e^{indq}.\end{gathered} \tag{D.6}$$

Substituting the Wannier state (Eq. D.5) into D.6, we obtain the obtain the formula for Bloch functions in Wannier states representation (invers transformation):

$$|\varphi_q^\nu>= \sqrt{\frac{d}{2\pi}} \sum_n e^{iqnd} |\Psi_n^\nu> . \tag{D.7}$$

The advantage of this representation for further calculations is that it has the q-dependence only in exponential part. Next, we put the Bloch states in the representation of Wannier states (Eq. D.7) into Eq. D.4, and obtain:

$$\begin{aligned} |\Phi_j^\nu>= \sqrt{\frac{d}{2\pi}} \int_{-\pi/d}^{\pi/d} dq\ exp\Big\{ -ijdq - i\Big(\frac{2T_1^\nu}{eFd}\Big) sin(qd)\Big\} \sqrt{\frac{d}{2\pi}} \sum_n e^{iqnd} |\Psi_n^\nu> \\ = \frac{d}{2\pi} \sum_n \int_{-\pi/d}^{\pi/d} dq\ exp\Big\{ i(n-j)dq - i\Big(\frac{2T_1^\nu}{eFd}\Big) sin(qd)\Big\} |\Psi_n^\nu> \\ = \frac{1}{2\pi} \sum_n \int_{-\pi}^{\pi} d\tau\ exp\Big\{ i(n-j)\tau - i\Big(\frac{2T_1^\nu}{eFd}\Big) sin(\tau)\Big\} |\Psi_n^\nu> . \end{aligned} \tag{D.8}$$

In Eq. D.8 we recognise the integral representation of Bessel function:

$$J_n(x) = \frac{1}{2\pi} \int_\pi^\pi d\tau\ e^{-i(n\tau - xsin(\tau))}. \tag{D.9}$$

Hence, after substituting Eq. D.9 into Eq. D.8 we come to the desired relation:

$$|\Phi_j^\nu>= \sum_n J_{n-j}\Big(\frac{2T_1^\nu}{eFd}\Big) |\Psi_n^\nu>, \tag{D.10}$$

what was to prove.

Bibliography

[1] L. Esaki, R. Tsu: *Superlattice and negative diferential conductivity in semiconductors*, IBM J. Res. Develop. 14, 61 (1970).

[2] M. Fornari, H.H. Chen, L. Fu, R.D. Graft, D.J. Lohrmann, S. Moroni, G. Pastori Parravicini, L. Resca, M.A. Stroscio: *Electronic structure and wave functions of interface states in HgTe-CdTe quantum wells and superlattices*, Phys. Rev. B 55, 24 (1997).

[3] J.M. Luttinger, W. Kohn: *Motion of Electrons and Holes In Perturbed Periodic Fields*, Phys Rev 97, 869 (1955).

[4] A. Wacker: *Semiconductor superlattices: a model system for nonlinear transport*, Phys. Rep. 357 (2002).

[5] D.J. BenDaniel, C.B. Duke: *Space-Charge Effects on Electron Tunneling*, Phys. Rev. 152, 683 (1966).

[6] M.E. Flatte, P.M. Young, L.H. Peng and H. Ehrenreich: *Generalized superlattice $K \cdot p$ theory and intersubband optical transitions*, Phys. Rev. B 53, 4 (1996).

[7] W. Kohn: *Analytic properties of Bloch waves and Wannier functions*, Phys. Rev. 115, 809 (1959).

[8] G. Nenciu: *Dynamics of band electrons in electric and magnetic fields: rigorous justification of the effective Hamiltonians*, Rev. Mod. Phys. 63, 91 (1991).

[9] E.O. Kane: *Zener tunneling in semiconductors*, J. Phys. Chem. Solids 12, 181 (1959).

[10] D.L. Smith, C. Mailhiot: *Theory of semiconductor superlattice electronic structure*, Rev. Mod. Phys. 62, 173 (1990).

[11] M. Glück, A.R. Kolovsky, H.J. Korsch, N. Moiseyev: *Calculation of Wannier-Bloch and Wannier-Stark states*, Eur. Phys. J. D 4, 239-246 (1998).

[12] J.R. Chelikowsky, M.L. Cohen: *Nonlocal pseudopotential calculations for the electronic structure of eleven diamond and zinc-blende semiconductors*, Phys. Rev. B 14, 556-582 (1976).

[13] N.F. Johnson, H. Ehrenreich, P.M. Hui, P.M. Young: *Electronic and optical properties of III-V and II-VI semiconductor superlattices*, Phys. Rev. B 41, 3655-3669 (1990).

[14] R.d.L. Kronig, W.G. Penney: *Quantum mechanics of electrons in crystal lattices* , Proc. Royal Soc. A 130, 499 (1931).

[15] A. Krier (ed.): *Mid-infrared Semiconductor Optoelectronics*, Springer-Verlag London (2006).

[16] G.H. Wannier: *Wave functions and effective Hamiltonian for Bloch electrons in an electric field*, Phys. Rev. 117, 432 (1960).

[17] L.R. Ram-Mohan, K.H. Yoo and R.L. Aggarwal: *Transfer-matrix algorithm for the calculation of the band structure of semiconductor superlattices*, Phys. Rev. B 38, 9 (1988).

[18] J. Zak: *Stark ladder in solids?*, Phys. Rev. Lett. 20, 1477-1381 (1968).

[19] L.L. Bonilla, and H.T. Grahn: *Non-linear dynamics of semiconductor superlattices*, Rep. Prog. Phys. 68, 577-683 (2005).

[20] C. Zener: *A Theory of Electrical Breakdown of Solid Dielectrics*, Roy. Soc. Lond. A 145 (1934).

[21] J.E. Avron, J. Zak, A. Grossmann, and L. Gunther: *Instability of the continuous spectrum: The N-band Stark ladder*, J. Math. Phys. 18, 918 (1977).

[22] G. Platero, R. Aguado: *Photon-assisted transport in semiconductor nanostructures*, Phys. Rep. 395, 1 (2004).